Stochastic Modeling and Simulation of DNA Electrophoretic Separation in a Microfluidic Obstacle Array

Aruna Mohan[†] and Patrick S. Doyle*

Department of Chemical Engineering, Massachusetts Institute of Technology, Cambridge, Massachusetts 02139

Received June 19, 2007; Revised Manuscript Received August 10, 2007

ABSTRACT: The size-dependent separation of electrophoresing DNA chains of varying lengths has recently been demonstrated to occur in microfluidic obstacle arrays. The chain dynamics in the array may be modeled as a continuous-time random walk, wherein the motion of the chain in the array is interspersed with collisions with the obstacles, involving a size-dependent random waiting time necessitated by the chain unraveling and unhooking following each collision. Previous studies employing the continuous-time random walk model do not fully account for the electric-field dependence of chain extension during collisions in the array. In this study, we extend the continuous-time random walk model of chain dynamics with account for incomplete chain extension. We evaluate the accuracy of the model by performing Brownian dynamics simulations of DNA chains of different lengths in a self-assembled array of magnetic beads at various electric field strengths and lattice spacings and provide comparisons between the predictions of the model and simulation results for the chain mobilities, dispersivities, mean collision probabilities, and the separation resolution achievable between different chain sizes in the device. We demonstrate that the model correctly predicts the nonmonotonicity of the separation resolution with respect to the electric field strength.

1. Introduction

The use of microfluidic post arrays for the size-based separation of electric-field driven DNA chains of different lengths, actuated by their size-dependent collisions with the posts, has recently been experimentally established. The size specificity of this technique owes itself to the fact that a longer chain requires more time for disentanglement following its collision with an obstacle than a shorter chain. The separation of DNA chains of various lengths in an obstacle array was first demonstrated by Volkmuth and Austin,[1] who employed obstacle courses fabricated in silicon via optical microlithography. More recently, Doyle et al.,[2] followed by Minc et al.,[3,4] have used self-assembled columns of superparamagnetic beads confined in a microfluidic channel, formed upon the imposition of a transverse magnetic field, to separate DNA chains of different lengths driven through the channel by the application of an electric field. Under conditions wherein the post spacing is larger than the chain sizes, separation in these devices relies on the formation of hooked chain configurations following collisions. Consequently, these devices may be used to separate long DNA chains. In contrast, the conventional separation technique of gel electrophoresis employs gels having a mean pore size smaller than the radii of gyration of the chains and relies on the reptation mechanism to achieve size separation. Under the application of a constant electric field, the chain mobility in the gel becomes independent of chain size for long chains, thereby imposing an upper limit of typically several tens of kilobase pairs on the chain lengths that can be separated via gel electrophoresis.[5] Thus, the use of microfluidic post arrays offers an advantage over gel electrophoresis. Post arrays have also been fabricated and employed under conditions such that the post spacing is comparable to the sizes of the chains to be separated.[6]

The chain dynamics in the obstacle array may be decomposed into three sequential, cyclically repeating steps,[7,8] namely, the collision of the chain with an obstacle and the unraveling of the two arms on either side of the obstacle, the unhooking of the chain, and the unhindered motion of the chain until its next collision with an obstacle. This process has been modeled by Minc et al.[7] as a nonseparable continuous-time random walk (CTRW) on a lattice.[9,10] The model of Minc et al. involves a random waiting time subsequent to a collision encompassing both the duration of the collision, namely, the time required for chain unraveling and unhooking, as well as the transit time at the free solution electrophoretic velocity between successive collisions.

Minc et al., following the analysis of Popelka et al.,[11] assumed the unraveling time for each arm of the chain to be proportional to the fraction of the chain represented by that arm. However, it has recently been established[12] that, upon modeling the post as a tether point during the unraveling process, the unraveling of the arms under conditions of strong field strengths occurs via a convective mechanism, whereby the transient arm length grows linearly in time at a rate equal to the free solution electrophoretic velocity and independent of its length. The analysis of Minc et al., therefore, overestimates the unraveling time and, hence, the duration of the collision. Another drawback of the analysis is that the collision probability at each obstacle was set equal to the areal post density, irrespective of the size of the chain. Moreover, Minc et al. equated the chain extension at the end of the unraveling process to the contour length of the chain, thereby neglecting its field-dependence. Consequently, their model failed to predict the experimentally observed field-dependence of the separation resolution.[3]

Recently, an attempt was made to take into account the incomplete extension of the chain during collisions at finite field strengths by Dorfman.[8] This study modeled the unraveling process as being equivalent to the unraveling of a tethered polymer chain in a uniform solvent flow field at a solvent velocity equal to the free solution electrophoretic velocity. With this assumption, use may be made of the results of Brochard-Wyart[13] relating the steady-state extension of a tethered chain

* Corresponding author. E-mail: pdoyle@mit.edu.
† E-mail: aruna@mit.edu.

10.1021/ma071354e CCC: $37.00
Published on Web 10/30/2007

to the solvent velocity, upon replacing the solvent velocity with the relative velocity of the solvent with respect to the extending chain arm, and solving for the rate of chain growth as a function of the instantaneous chain length, under the assumption of quasisteady stretching. The relationship between chain extension and solvent velocity at steady-state provided by Brochard-Wyart[13] is expressed in eq 12 of ref 8, wherein the symbol "v" may be associated with the solvent velocity relative to the rate of chain growth (namely, $\mu_0 E - \mathrm{d}L_1/\mathrm{d}t$ in the notation of ref 8). However, the symbol "v" in eqs 5 and 6 of ref 8 refers to the rate of extension of the long arm of the chain (or in dimensional notation, $\mathrm{d}L_1/\mathrm{d}t$). The study of ref 8 subsequently assumes equivalence of the relationship between the steady-state chain extension and the free solution electrophoretic velocity and that between the transient chain extension and its rate of growth, thereby rendering invalid the analysis of ref 8.

The development of a more accurate model of chain dynamics in an obstacle array requires knowledge of chain−obstacle interactions during and subsequent to a collision. Several studies have focused on the mechanism of collision of a chain with a single, stationary obstacle. Nixon and Slater[14] have provided a rope-over-pulley model of chain unhooking, assuming Gaussian and uniform distributions of the initial difference in arm lengths on either side of the obstacle following a collision. These authors have found that the mean and variance of the unhooking time exhibit the same scaling dependence on the chain length regardless of the initial distribution of arm lengths. A strong dependence of the collision probability and the duration of a collision on the impact parameter has been demonstrated in refs 15 and 16. More complicated configurations involving the hooking of a single chain around two or more obstacles have been theoretically studied in ref 17.

More recently, as described in a series of papers, Randall and Doyle[18−20] have provided detailed experimental investigations of polymer−obstacle collisions in PDMS microchannels enclosing an obstacle or a dilute array of obstacles and have proposed physical mechanisms for the dynamics of chain unraveling and unhooking subsequent to a collision. These authors have classified polymer−obstacle collisions into J- or U-collisions (according as the initial lengths of the two arms of the chain are unequal or equal) involving the sequential unraveling and ropelike unhooking of the two arms of the chain, X-collisions, wherein the long arm of the chain continues to unravel as the chain is unhooking from the post, and rare, metastable W-collisions, resulting from the formation of entangled chain configurations.[20] Different models were proposed for the unhooking time and the holdup time during which the center of mass motion is obstructed by the obstacle following X- and J-collisions, inspired by the distinct mechanisms operative in the two cases. X-collisions were found to occur predominantly under conditions of strong electric fields or, equivalently, at high Peclet numbers. These findings were corroborated by the simulation study of Kim and Doyle,[21] based on Brownian dynamics simulations of collisions of λ-, 2λ-, and T4-DNA with a single post. The latter study revealed that a crossover from the predominance of X-collisions to J-collisions occurs at an initial short arm fraction of approximately 0.4, with X-collisions being predominant at initial short arm fractions below this value. Kim and Doyle further provided comparisons of the unhooking time and center of mass holdup time as predicted by the collision models of ref 20 with simulation data. In accord with the experimental observations of ref 20, it was discovered that the ropelike unhooking time of a chain at constant extension provides an excellent approximation of the center of mass holdup time during a polymer−obstacle collision for the entire range of field strengths and chain lengths studied for both X- and J-collisions. Although the holdup times for W-collisions observed in simulations differed from the predicted holdup times of the X- and J-models, as well as from the ropelike unhooking time, such collisions are rare and may be neglected. Furthermore, Kim and Doyle also observed the probability distribution of the initial short arm fraction to be increasingly well-approximated by a uniform distribution as the field strength is increased.

In the present study, we make use of the insight gained into chain−obstacle collisions from the aforementioned studies to develop a more accurate CTRW model of chain dynamics in the array. The center of mass holdup time following each collision is well-approximated by the ropelike unhooking time, as described in the preceding paragraph. We employ the low-force and large-force limits of the Marko−Siggia interpolation formula for the wormlike chain,[22] which best describes DNA elasticity, to derive the dependence of chain extension on the field strength.[21] Furthermore, we account for the dependence of the collision probability at each obstacle on the chain size. Concomitantly, we perform Brownian dynamics simulations of DNA chains of three sizes, namely, λ-DNA and the two shorter chains λ/3-DNA and 2λ/3-DNA resulting from its digestion with the restriction enzyme Xho I,[2] in microfluidic post arrays formed from the self-assembly of magnetic beads.[23,24] We analyze the shortcomings of the model in light of the results for chain mobility, dispersivity, collision probability, mean distance covered between successive collisions, and the separation resolution obtained from simulation.

The paper is organized as follows. In section 2, we present the revised CTRW model. Section 3 details our simulation methods, while in section 4, we provide comparisons between model predictions and simulation results and evaluate the performance of the model. Section 5 provides a summary of our findings.

2. CTRW Model of Chain Dynamics

In this section, we briefly describe the main features of the revised CTRW model of DNA motion in the obstacle array. The chain is modeled as a random walker commencing from position $r = 0$ and moving in the field direction at the free solution electrophoretic velocity $\mu_0 E$ between successive collisions, with μ_0 the free solution electrophoretic mobility and E the magnitude of the electric field strength. When a collision occurs at an obstacle, the chain waits at the location $r = na$ of the obstacle during the unraveling and unhooking processes before continuing at the free solution electrophoretic velocity until the next collision, where a denotes the lattice constant and n is an integer. We denote by τ_H the holdup time[20] during which the center of mass motion is obstructed by the obstacle, which we approximate by the expression

$$\tau_H = -\frac{\mathscr{L}}{2\mu_0 E}\ln(1 - 2r_0) \qquad (1)$$

representing the ropelike unhooking time of a chain at constant extension, with r_0 the initial fraction of the chain contained in the short arm and $\mathscr{L}$ the total chain extension at the start of the unhooking process. Equation 1 has been found to provide an excellent approximation to the holdup time for a wide range of chain lengths and field strengths.[21] The short arm fraction at the start of each collision, $r_0 = x_1(0)/\mathscr{L}$, with $x_1(0)$ the short arm length at the start of the unhooking process, is assumed to be uniformly distributed in the interval [0, 0.5]. The assumption

of a uniformly distributed initial short arm fraction has been found to hold at high field strengths.[21] The use of other distributions at low field strengths, such as the Gaussian distribution, may have a quantitative effect on the results.[14]

The transition time taken to move from the start of one chain−obstacle collision to the next is now computed as the sum of the holdup time τ_H and the transit time until the next collision occurring a distance $r = na$ away, i.e.,

$$\tau = \tau_H + \frac{na}{\mu_0 E} \tag{2}$$

Following Minc et al.,[7] we assume that no collisions occur along the extended backbone of the chain and set the probability $h(n)$ that successive collisions are separated by n lattice columns to be

$$h(n) = \begin{cases} \rho(1-\rho)^{n-n^*} & \text{if } n \geq n^* \\ 0 & \text{otherwise} \end{cases} \tag{3}$$

where ρ is the collision probability at any obstacle and n^* is the first lattice position at which the next collision can occur, given by the expression[7]

$$n^* = \frac{\mathscr{L}}{a} \tag{4}$$

Note that the mean distance covered between successive collisions obtained from eq 3 is

$$a\langle n \rangle = a\left(\frac{1-\rho}{\rho} + n^*\right) \tag{5}$$

Equations 1−3, taken in conjunction with the assumption that r_0 is uniform in the interval [0, 0.5], enable the computation of the transition probability density function for making a transition between successive collisions separated by a given number of lattice columns in a specified time duration. Knowledge of the transition probability density next enables the calculation of the probability density $p(r,t)$ of the position $R(t)$ of the random walker at time t. For this purpose, we adopt the CTRW model on a discrete lattice developed by Scher and Lax[9,10] and employed previously by Minc et al.[7] and Dorfman.[8] The reader is referred to the aforementioned studies for details. The long time asymptotic mean velocity U and dispersivity D of the walker are related as usual for diffusion processes to the mean and variance of the random walker's position $R(t)$ in the long time limit of $t \to \infty$. We omit the tedious but straightforward algebraic details and simply provide the results below:

$$\frac{\mu}{\mu_0} = \frac{2(1-\rho+\rho n^*)}{3\rho n^* + 2(1-\rho)} \tag{6}$$

and

$$\frac{D}{\mu_0 E a} = \frac{n^{*2}\rho\,[2+\rho(2n^*-3)+\rho^2(n^*-1)^2]}{[3\rho n^* + 2(1-\rho)]^3} \tag{7}$$

where we have introduced the mobility μ via the relation $U = \mu E$.

The Scher−Lax model[9] assumes that, following a collision, the random walker waits at the lattice site representing the obstacle position for the entire duration of the transition time and instantaneously makes a jump to the next lattice site at the end of the transition time period. This model has been variously referred to as the leaper model[10] or the jump model.[25] In reality, the DNA molecule moves at approximately the free solution electrophoretic velocity between successive collisions. A CTRW model wherein the random walker moves at a constant velocity between successive turning points, referred to as the creeper model[10] or the velocity model,[25] has been previously proposed. Although both models are known to exhibit the same asymptotic behavior, they may differ by a numerical constant.[10,25] However, the form of the transition probability density used in the present study (as well as in refs 7 and 8) decays exponentially for large values of the transition time, rendering the long time behavior of the moments of the walk insensitive to the type of model used.[10]

The collision probability ρ and the field-dependence of the chain extension $\mathscr{L}$ at the start of unhooking remain to be specified. We postulate that ρ may be approximated by the expression

$$\rho = \frac{R_g}{a} \tag{8}$$

where R_g is the radius of gyration of the chain. Equation 8 attempts to account for the dependence of the collision probability on the chain size and is expected to be best-suited to situations wherein the post diameter is small compared to the coil size, which in turn is small compared to the lattice constant, under the assumption that the chain instantaneously relaxes to its equilibrium coil shape following a collision. We, however, make use of eq 8 even in situations wherein the chain radius of gyration is comparable to the post radius.

The chain extension will be derived from the low- and large-force limit of the Marko−Siggia formula in the regime of weak and strong stretching, respectively. The former, Gaussian regime derives from the Marko−Siggia rule in the limit $\mathscr{L}/L \ll 1$, while the latter corresponds to the limit $\mathscr{L}/L \lesssim 1$, where L denotes the contour length of the chain. The crossover from weak stretching to strong stretching occurs at $\mathrm{Pe}_{\mathrm{chain}} \sim 1$,[12] where we have introduced the Peclet number

$$\mathrm{Pe}_{\mathrm{chain}} = \frac{\mu_0 E \zeta_{\mathrm{chain}} A}{k_B T} \tag{9}$$

In eq 9, ζ_{chain}, A, and $k_B T$ refer, respectively, to the drag coefficient for the chain, the persistence length of double-stranded DNA (known to be 53 nm), and the thermal energy. Note that eq 9 represents the nondimensional drag force acting on the chain, whereby the value $\mathrm{Pe}_{\mathrm{chain}} \sim 1$ delineates the regimes of weak and strong chain stretching.[12] The Marko−Siggia interpolation rule then yields

$$\mathscr{L} = \begin{cases} \frac{L}{6}\mathrm{Pe}_{\mathrm{chain}}, & \mathrm{Pe}_{\mathrm{chain}} \leq 1 \\ L(1-\mathrm{Pe}_{\mathrm{chain}}^{-1/2}), & \mathrm{Pe}_{\mathrm{chain}} > 1 \end{cases}$$

where an effective force equivalent to $^1/_4$ of the drag force $\mu_0 E \zeta_{\mathrm{chain}}$ has been employed to account for the nonuniformity in drag along the chain.[21,22] As intimated by eq 10, the dependence of the chain extension on the Peclet number is deduced from the Marko−Siggia interpolation formula under the assumption that a sharp transition from weak to strong stretching occurs at $\mathrm{Pe}_{\mathrm{chain}} = 1$, although no such sharp transition occurs in reality. We have verified that the results are hardly

affected upon instead assuming the transition to occur at $Pe_{chain} = 2$, corresponding to roughly 30% chain extension.

Equations 6 and 7 may now be substituted in the expression[7]

$$R_s = \frac{|U_1 - U_2|}{U_1 + U_2}\sqrt{\frac{L_s}{16}\left(\frac{U_1}{D_1} + \frac{U_2}{D_2}\right)} \tag{10}$$

for the separation resolution R_s, where the subscripts 1 and 2 refer to the two species to be separated, and L_s is the separation length.

3. Brownian Dynamics Simulations

3.1. Chain Simulations. We adopt the technique of Brownian dynamics applied to the bead−spring model of the chain to simulate its behavior in a post array. Brownian dynamics is based on the application of the Langevin equation

$$d\mathbf{r}_j = \left[\mu_0\mathbf{E} + \frac{1}{\zeta}(\mathbf{F}_j^s + \mathbf{F}_j^{ev})\right]dt + \sqrt{\frac{2k_BT}{\zeta}}d\mathbf{W}_j, \quad j = 1, .., N \tag{11}$$

to each bead $j = 1, .., N$ of the chain, where $\mathbf{r}_j$ denotes the position vector of bead j relative to the origin, while $\mathbf{F}_j^s$ and $\mathbf{F}_j^{ev}$ refer, respectively, to the spring force exerted on bead j by the adjoining springs and the net excluded volume force exerted on bead j by the remaining beads. The distortion of the electric field $\mathbf{E}$ caused by the presence of finite-size, nonconducting posts is neglected. The force exerted on the negatively charged DNA chain by the electric field is accounted for via the inclusion of the term $\mu_0\mathbf{E}$ in eq 11.[26] Contrary to convention, we assign the direction of $\mathbf{E}$ to that of the electric force experienced by a negative test charge, so that μ_0 is positive. Free draining conditions are assumed, and the drag coefficient for a single bead, given by Stokes' law, is denoted by ζ, whereby $\zeta_{chain} = N\zeta$. The term $\mathbf{W}_j$ represents a three-dimensional Wiener process, with $\langle d\mathbf{W}_j(t)\rangle = 0$ and $\langle d\mathbf{W}_j(t)d\mathbf{W}_k(t')\rangle = dt\delta_{jk}\delta(t - t')\boldsymbol{\delta}$, where $k = 1, .., N$ and $\boldsymbol{\delta}$ is the identity tensor. The x-coordinate is measured along the direction of the electric field $\mathbf{E}$.

We consider DNA molecules of three lengths, namely, λ-DNA (having 48 502 base pairs with a contour length of 20.5 μm when stained with YOYO dye in the ratio of 4 base pairs of DNA per molecule of dye) and the two fragments 2λ/3-DNA (containing 33 497 base pairs) and λ/3-DNA obtained from the digestion of λ-DNA with the restriction enzyme Xho I.[2] We adopt the discretization used by Kim and Doyle to model λ-DNA[21] and select $N_{k,s} = 5.23$ Kuhn lengths per spring, with the Kuhn length $b_k = 0.106$ μm being equivalent to two persistence lengths. At this discretization, used in conjunction with a sufficiently small time step as described later in this section, we are assured that aphysical configurations, wherein the chain appears to intersect an obstacle, are forbidden from arising. Concurrently, use of this discretization offers a compromise between ensuring an acceptable computational speed and providing an adequately fine-grained description of the chain. We, therefore, select $N = 38$ beads to model λ-DNA, whereas 2λ/3-DNA and λ/3-DNA are modeled by $N = 27$ and $N = 12$ beads, respectively. The corresponding chain lengths of 2λ/3-DNA and λ/3-DNA, 14.4 μm and 6.1 μm, respectively, differ slightly from the values 14.2 μm and 6.3 μm, respectively, estimated by assuming a linear dependence of the contour length on the number of base pairs.

We perform simulations at a number of experimentally accessible field strengths expressed in terms of a Peclet number as defined by eq 9, with Pe_λ, based on the value $N = 38$ selected for λ-DNA, varying from 0.1 to 50. The corresponding values of Pe_{chain} for 2λ/3-DNA and λ/3-DNA are obtained by means of the equality $Pe_{chain} = Pe_\lambda N_{chain}/38$, where N_{chain} is the number of beads modeling the chain of interest. This range of values corresponds to electric field strengths ranging from 0.5 to 100 V/cm, estimated from eq 9 for a λ-DNA molecule having a radius of gyration of 0.69 μm and a thickness of 2 nm[27] at $T = 298$ K in a solvent of viscosity 1 cP by making use of the Zimm drag coefficient for a coil at $Pe_\lambda = 0.1$ and the drag coefficient for a rod at $Pe_\lambda = 50$,[28] and using the experimentally measured value of μ_0.[3] In addition, for λ-DNA, we also provide data for chain dispersivity at $Pe_\lambda = 0.01$ and 0.05.

The elasticity of DNA is characterized by the wormlike chain model, the force−extension behavior of which is described by the interpolation formula due to Marko and Siggia,[22] modified by Underhill and Doyle[29] by the introduction of an effective persistence length in place of the true persistence length. Following Kim and Doyle,[21] we adopt the modified Marko−Siggia law and employ the ratio 1.91 of the effective persistence length to the true persistence length deriving from the low force criterion of Underhill and Doyle.[29] We model intrachain exclusion by means of the soft, repulsive force proposed by Jendrejack et al.,[30] given by the expression

$$\mathbf{F}_j^{ev} = \upsilon k_BTN_{k,s}^2\pi\left(\frac{3}{4\pi S_s^2}\right)^{5/2}\sum_{k=1,k\neq j}^{N}\exp\left[-\frac{3}{4S_s^2}\left|\mathbf{r}_j - \mathbf{r}_k\right|^2\right](\mathbf{r}_j - \mathbf{r}_k) \tag{12}$$

where υ is the excluded volume parameter and $S_s^2 = N_{k,s}b_k^2/6$ the mean equilibrium size of a Gaussian spring of $N_{k,s}$ Kuhn segments. We employ the value $\upsilon = 0.0004$ μm^3, determined by Kim and Doyle to accurately reproduce the radius of gyration of λ-DNA. With the above parameters, the equilibrium radii of gyration obtained from simulations of 2λ/3-DNA and λ/3-DNA in free solution are 0.59 μm and 0.37 μm, respectively, which are close to the values 0.56 μm and 0.34 μm obtained from the good solvent scaling law $R_g \sim L^{0.589}$.[31]

We consider channel heights large compared to the size of the chain[3] and ignore interactions between the beads and the channel walls. As a result, the dynamic behavior of interest to us is confined to the two dimensions spanning the channel plane. The interactions between the chain and the obstacles in the array are modeled by hard-sphere exclusion implemented via the Heyes−Melrose algorithm,[32] whereby an overlap between a bead and an obstacle resulting from the integration of eq 11 at any time point is subsequently corrected by displacing the bead along the line of centers until the bead and the obstacle are just touching. The beads are modeled as having no hard-sphere volume.[21] Since hard-sphere exclusion is implemented independent of time stepping, the possibility exists that a spring may be overstretched as a result of its implementation. This problem is alleviated by using sufficiently small time steps. Simultaneously, the time step must also be small compared to the relaxation time of a single spring. At a Peclet number below 0.1 for each chain, a time step of $0.01\zeta Q_0^2/(k_BT)$, with Q_0 the maximum spring length, was found to suffice, with the time step at stronger field strengths chosen to be inversely proportional to the Peclet number. Under these conditions, overstretching is largely eliminated. In the extremely rare instances when overstretching occurred (in fewer than a millionth of the total number of time steps for a typical trajectory), the spring force was calculated by linearly extrapolating the modified Marko−Siggia force law from the value of the force at 99% spring extension.

We adopt the semi-implicit predictor−corrector scheme described in ref 28 for the integration of eq 11. Averages are performed over an ensemble of between 100 and 1000 chains. The array geometries employed are described in section 3.2. Initial equilibrium configurations are generated by employing the Marko−Siggia force law to simulate the evolution to equilibrium of initially Gaussian coils.[12] These coil configurations are placed upstream of the array at the start of the simulation and are subsequently stretched and deformed from their initial coil shape owing to collisions, resulting in an initial increase in chain stretch. Subsequently, the stretch equilibrates, fluctuating about a steady mean value. A time duration corresponding to the time taken to cross a distance of 50−100 lattice spacings at the free solution electrophoretic velocity is found sufficient to ensure equilibration. Subsequently, the equilibrated chain is simulated further in the array for the same time duration.

The long time mean velocity and dispersivity are obtained from the mean and variance of the distribution of the center of mass x-coordinates (denoted x_{cm}) for an ensemble of chains at the end of the simulation, measured relative to their values at the end of the equilibration process, by fitting to a normal distribution and using the relations $\langle x_{cm}\rangle = Ut$ and $\mathrm{var}(x_{cm}) = 2Dt$, where t is the time duration of the simulation following the equilibration process. In all cases, the assumption of normality is confirmed by performing the Kolmogorov−Smirnov test.[33] Additionally, we define a collision to have occurred when a portion of the chain is present in all four quadrants of a coordinate plane whose origin lies at the obstacle center,[20,21] and enforce the conditions that a collision with a given obstacle occur only once per trajectory, and (although the situation did not arise in our simulations) that a collision at a given time step with multiple obstacles be counted as a single collision. We deduce the mean probability of collision at each obstacle from simulation by dividing the number of collision events occurring in a trajectory by the number of lattice spacings covered by the chain center of mass in that trajectory following equilibration, averaged over the ensemble. We also measure the mean distance covered by the chain center of mass between successive collisions in each trajectory after equilibration, averaged over the ensemble, while excluding trajectories in which fewer than two collisions occur in performing the ensemble-average. We note that this exclusion of trajectories, arising from our inability to account for the effectively infinite distance between collisions observed in trajectories involving a single collision or no collisions, may adversely impact our prediction of the mean distance covered between collisions, as pointed out in section 4.

3.2. Selection of Array Geometries. We chose a hexagonal geometry as being representative of the lattice pattern resulting from the self-assembly of magnetic colloids[23,24] and conducted an initial set of simulations of λ-DNA in a planar, semi-infinite hexagonal array occupying the right-half plane $x \geq 0$, composed of obstacles of diameter $d = 1$ μm at a lattice constant of $a = 3$ μm. The array orientation was such that the separation between adjacent lattice points along the x-axis was equal to the lattice constant. Hard-sphere exclusion between the chain and the obstacles was enforced by exploiting the regularity of the lattice to identify the obstacles in the vicinity of each bead of the chain at every time step. Figure 1 illustrates the results of these simulations. It is clear from Figure 1 that the obstacles in a regular, dilute lattice provide straight channels through which the chain can pass without hindrance, and the normalized mobility and normalized dispersivity of the chain rapidly

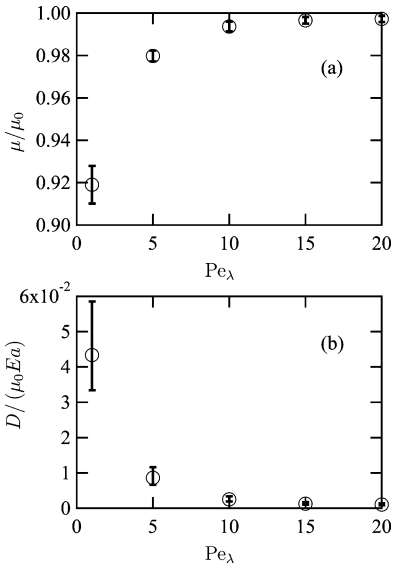

Figure 1. (a) Normalized mobility and (b) dispersivity of λ-DNA as a function of Pe_λ calculated from simulation in a regular hexagonal array having a lattice constant of 3 μm.

asymptote to 1 and 0, respectively, as the Peclet number is increased. This observation is consistent with the finding of Patel and Shaqfeh[34] that disordered post arrangements are essential for separation.

We were motivated by the above finding to employ an array more representative of a magnetic colloid assembly, generated via free draining Brownian dynamics simulations of a collection of hard spheres, each of diameter $d = 1$ μm, with repulsive point dipoles at their centers in two dimensions, with a magnetic field applied normal to the plane, and with the neglect of mutual induction between the colloids.[23,24] The magnetic particles are confined to the portion of the $x-y$ plane bounded by $x = 0$, $x = X$, $y = 0$, and $y = Y$ by means of periodic boundary conditions. X and Y, denoting the length and width of the periodically repeating unit constituting the semi-infinite, planar array occupying the region $x \geq 0$, are chosen to be 600.1 and 129.9 μm, respectively. The initial condition corresponds to a perfect hexagonal lattice, with four times as many particles placed along the x-axis as along the y-axis. This condition, in conjunction with the ratio $Y/X = \sqrt{3}/8$ of the unit cell dimensions, was chosen to yield an array orientation such that the separation between adjacent lattice points along the x-axis was equal to the lattice constant.

The dimensionless interaction energy for the magnetic colloid system is defined as[23,24]

$$\Gamma = \frac{\Lambda}{2}\left(\frac{d}{R}\right)^3 \tag{13}$$

where $R = a\sin(\pi/3)$, a denotes the lattice spacing, and Λ is the ratio of the interaction potential between two dipoles oriented parallel to each other and separated by a distance d, to the thermal energy.[23,24] All two-dimensional systems at the same value of Γ behave identically if R is the only relevant length scale in the system, provided that the system size is large enough that finite size effects are negligible.[23,24] We chose the value $\Gamma = 12$, at which the lattice possesses neither translational nor long-range orientational order and, hence, lies in the liquid phase. The value of Γ was held constant at 12, and the number of colloids N_c in the unit cell and Λ were varied in order to vary the lattice spacing while holding fixed the remaining lattice characteristics, by means of the relation $a = [\sqrt{3}N_c/(2XY)]^{-1/2}$.[23,24] In all simulations, pairwise dipole−

dipole interactions were considered only between pairs of particles separated by a distance less than a cutoff of 7*R*. The simulations were run until the defect concentration reached steady state,[24] at a time step of approximately $10^{-3}\zeta' d^2/(k_B T)$, where ζ' is the drag coefficient for each magnetic colloid. Following the attainment of steady state, the positions of the magnetic colloids were held constant and were not allowed to evolve further once the chain was introduced in the array. The reader is referred to refs 23 and 24 for further details on the simulation methods adopted for magnetic colloid systems and their characteristics.

We employ assemblies of $N_c = 40\,000$, 10 000, 4900, 2500, 1600, and 900 colloidal particles, yielding mean lattice spacings averaged over nearest-neighbor pairs[23,24] of 1.53, 3.06, 4.37, 6.12, 7.65, and 10.21 μm, respectively. The corresponding defect concentrations (where a defect is defined as a particle with greater or fewer than six nearest neighbors) are 0.306, 0.301, 0.292, 0.307, 0.311, and 0.332, respectively. The slight increase in defect concentration for the system containing $N_c = 900$ particles may be the result of finite size effects associated with the relatively small size of the system. However, finite size effects are not significant at $\Gamma = 12$, which is sufficiently far from the phase boundary.[23,24] The assembly having a mean lattice spacing of $a = 3.06$ μm is employed to study the behavior of the chain at varying field strengths. This lattice is illustrated in Figure 2, which provides a comparison between a regular hexagonal lattice and the former quasi-regular array of magnetic colloids as well as an experimentally generated lattice of magnetic colloids from the study of Doyle et al.[2] In studies where the mean lattice spacing is varied, the field strength is held constant at its value corresponding to $Pe_\lambda = 5$.

Upon the introduction of the chain in the array, the implementation of hard-sphere chain−obstacle exclusion and the identification of hooked chain configurations require that a search be performed over obstacles at each time step. This is facilitated by binning the obstacles in the unit cell at the start of the simulation via a linked list implementation of neighbor lists within each bin.[35] The bin dimensions are chosen to be comparable to the mean lattice spacing. Periodic boundary conditions are imposed on the chain at the boundaries of the unit cell by periodically reconstructing the unit cell in the vicinity of the chain. Subsequently, chain−obstacle overlaps may be detected by searching only the bin containing the position of each bead of the chain and the eight surrounding bins, and similarly, hooked chain configurations may be identified by searching only the bins enclosed by the maximum and minimum chain coordinates.

The results of our simulations in the self-assembled magnetic colloid arrays are described in section 4.

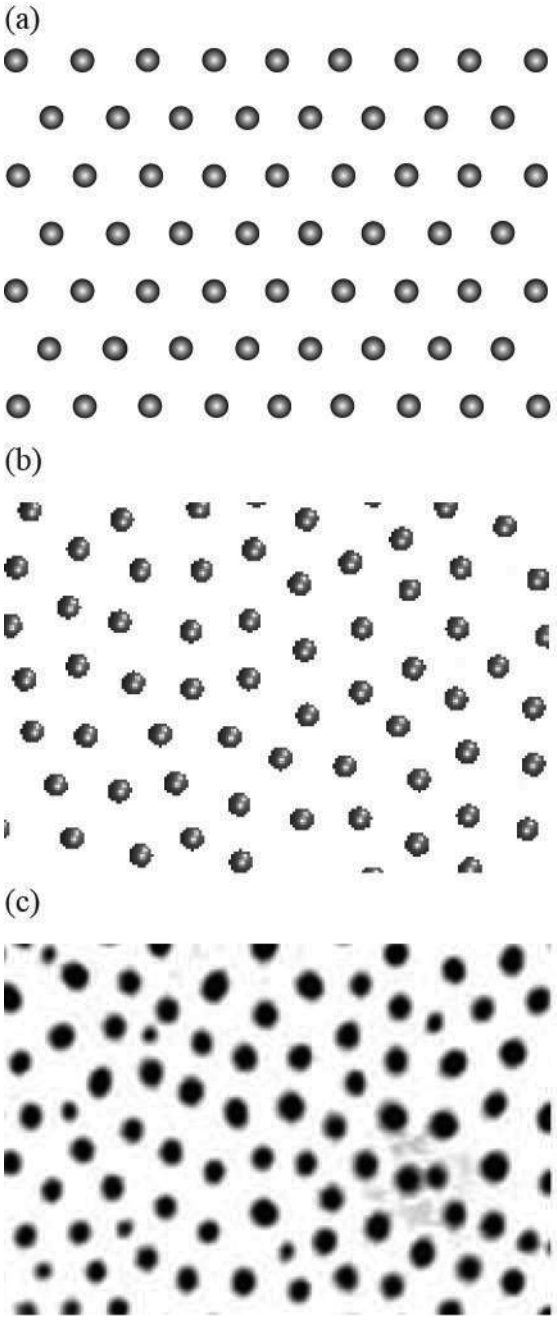

Figure 2. (a) A regular hexagonal lattice, (b) a portion of a self-assembled array of magnetic beads having a mean lattice spacing of 3.06 μm, and (c) a portion of an experimentally generated self-assembled array of magnetic beads,[2] corresponding to a section of width 40 μm.

4. Comparison of Model Predictions and Simulation Results

4.1. Varying Field Strengths. Figures 3−5 provide comparisons between the normalized mobility and dispersivity and the mean distance covered between successive collisions obtained from simulations and those predicted by the CTRW model for the three chain lengths studied at various field strengths at a fixed mean lattice spacing of 3.06 μm. Furthermore, Figure 6 provides a comparison between the mean collision probability observed in simulations and those assumed in the present CTRW model, i.e., R_g/a, and in the study of Minc et al., i.e., d/a. The mobility is normalized with respect to its free solution value μ_0 and the dispersivity with respect to $\mu_0 Ea$. The error bars for the mobility and dispersivity are obtained from the 95% confidence limits for the mean and variance upon fitting the distribution of center of mass *x*-coordinates at the end of the simulation relative to their equilibrated values to a normal distribution.[33] Similarly, the error bars for the mean distance covered between collisions and the mean collision probability represent 95% confidence limits for the means of the respective distributions, again upon fitting to a normal distribution. The predictions of the CTRW model for the normalized mobility and dispersivity derive from eqs 6 and 7, respectively, taken in conjunction with eqs 4 and 8−10. The mean distance between collisions following from the CTRW model is stated in eq 5.

The simulation data depicted in Figures 3−6 enable the identification of three regimes delineated by the Peclet number

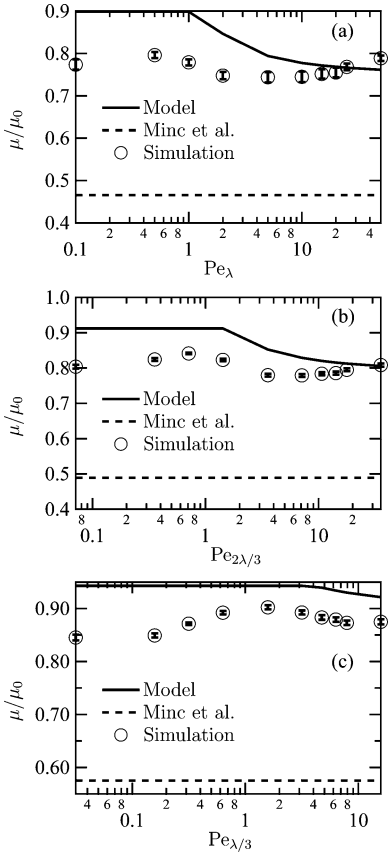

Figure 3. Normalized mobility of (a) λ-DNA, (b) $2\lambda/3$-DNA, and (c) $\lambda/3$-DNA as a function of the Peclet number for λ-, $2\lambda/3$-, and $\lambda/3$-DNA, respectively, obtained by simulation in a self-assembled array of magnetic beads having a mean lattice spacing of 3.06 μm (○), that predicted by the model (—), and that predicted by the model of Minc et al. (- - - -). The error bars represent 95% confidence bounds on simulation results.

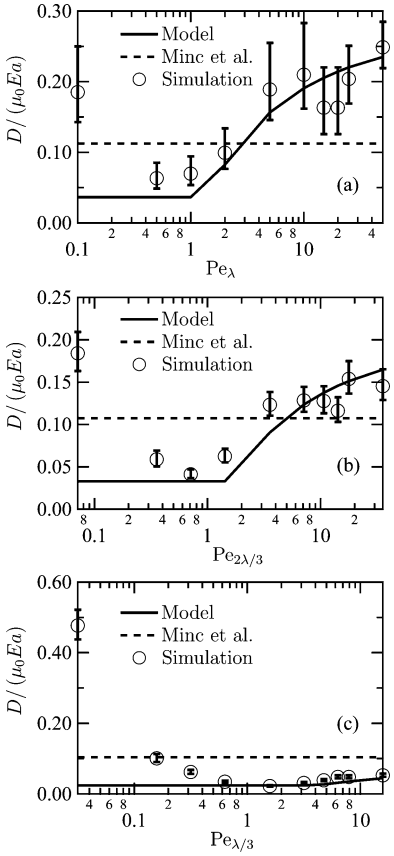

Figure 4. Normalized dispersivity of (a) λ-DNA, (b) $2\lambda/3$-DNA, and (c) $\lambda/3$-DNA as a function of the Peclet number for λ-, $2\lambda/3$-, and $\lambda/3$-DNA, respectively, obtained by simulation in a self-assembled array of magnetic beads having a mean lattice spacing of 3.06 μm (○), that predicted by the model (—), and that predicted by the model of Minc et al. (- - - -). The error bars represent 95% confidence bounds on simulation results.

for the chain, namely, (i) $Pe_{chain} < O(A/R_g)$, (ii) $O(A/R_g) < Pe_{chain} \lesssim O(1)$, and (iii) $Pe_{chain} \gg O(1)$. Below, we investigate the physical mechanisms operative in these three regimes.

The transition occurring at $Pe_{chain} \sim O(1)$ was encountered earlier in eq 10 and corresponds to the transition from the regime of weak stretching to strong stretching. For $Pe_{chain} \lesssim O(1)$, the chain is in the near-equilibrium, Gaussian regime and its elasticity is well-described by linear Hooke's law behavior, corresponding to the limit $\mathcal{L}/L \ll 1$ of the Marko−Siggia law. However, as the Peclet number is increased, the behavior of the chain is increasingly dominated by its finite extensibility and for $Pe_{chain} \gg O(1)$, we approach the opposite limit $\mathcal{L}/L \lesssim 1$.[12]

Figures 3 and 5 reveal the existence of minima in the chain mobility and the mean distance covered between successive collisions at an $O(1)$ value of Pe_{chain}. These minima correspond well with the occurrence of a maximum in the collision probability at an $O(1)$ value of Pe_{chain}, as seen in Figure 6. The existence of a minimum in the chain mobility at an $O(1)$ value of the chain Peclet number was also noted by Patel and Shaqfeh in their study of chain dispersion in random arrays.[34] These authors have interpreted the chain Peclet number as representing the ratio of the escape time for the chain to diffuse away from the obstacle to the hairpin formation time. The time scale R_g^2/D_{chain} [with $D_{chain} = k_BT/(N\zeta)$] for center of mass diffusion over a distance equal to the equilibrium chain radius represents a time scale for escape, enabling the chain to diffuse away from the obstacle and, hence, avoid hooking, while a time scale of $L/(\mu_0 E)$ represents a time scale for the unraveling of the chain arms and may be identified with the time of formation of a hooked chain configuration. As the ratio of the former to the latter, $\mu_0 E/D_{chain}(R_g^2/L) \sim Pe_{chain}$, increases to an $O(1)$ value, the probability of hooking collisions increases. We caution that the identification of Pe_{chain} with the aforementioned ratio of time scales is strictly valid only in a Θ solvent. Upon taking account of the intrachain exclusion arising under good solvent conditions, a weak dependence on the chain length appears in the scaling relation $\mu_0 E/D_{chain}(R_g^2/L) \sim N_k^{0.2} Pe_{chain}$, deriving from the scaling law $R_g^2 \sim N_k^{1.2} b_k^2$ for a self-avoiding walk of N_k Kuhn steps.[31] However, for the chain sizes presently under consideration, $N_k \sim 100$ and, consequently, $N_k^{0.2} \sim 1$, whereby our conclusions remain valid.

In consequence of the preceding scaling arguments, the probability of forming a hooked, hairpin configuration upon encounter with an obstacle initially increases as the Peclet number increases to approach an $O(1)$ value. However, as the Peclet number is further increased beyond a value of 1, the chain becomes highly stretched during collisions and the cross-sectional area subsequently presented to the obstacles decreases. As a result, the collision probability decreases, and the mobility and mean distance covered between collisions increase as the Peclet number is increased beyond $O(1)$ values. The location of these extrema is shifted to higher values of Pe_{chain} in the case of $\lambda/3$-DNA, possibly owing to finite size effects arising in shorter chains.

We next consider the behavior of the chain at Peclet numbers of the order of A/R_g or, equivalently, 0.1 for the chain sizes

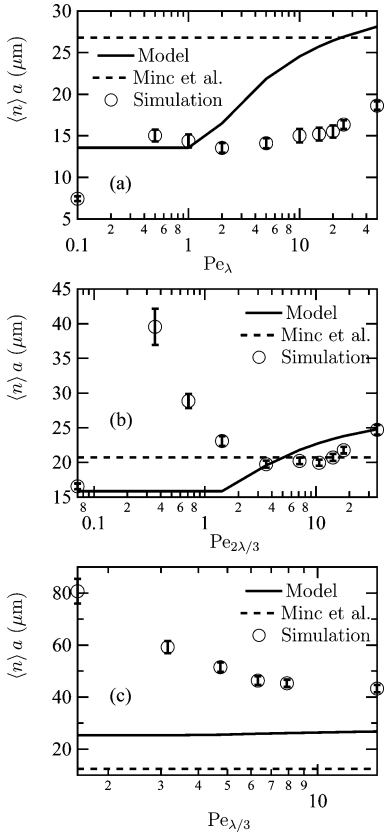

Figure 5. Mean distance $\langle n \rangle a$ covered between successive collisions by (a) λ-DNA, (b) $2\lambda/3$-DNA, and (c) $\lambda/3$-DNA as a function of the Peclet number for λ-, $2\lambda/3$-, and $\lambda/3$-DNA, respectively, obtained by simulation in a self-assembled array of magnetic beads having a mean lattice spacing of 3.06 μm (○), that predicted by the model (—), and that predicted by the model of Minc et al. (- - - -). The error bars represent 95% confidence bounds on simulation results. The simulation data shown for $\lambda/3$-DNA correspond to $\mathrm{Pe}_{\lambda/3} = 1.58$ and higher only, since collisions were observed to occur in fewer than 10% of the simulated trajectories at lower field strengths.

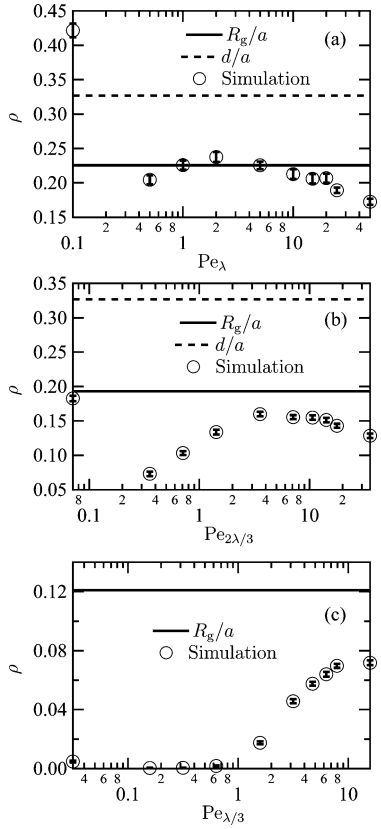

Figure 6. Mean collision probability ρ of (a) λ-DNA, (b) $2\lambda/3$-DNA, and (c) $\lambda/3$-DNA, calculated as the number of chain−obstacle collisions per lattice column crossed by the chain center of mass, as a function of the Peclet number for λ-, $2\lambda/3$-, and $\lambda/3$-DNA, respectively, obtained by simulation in a self-assembled array of magnetic beads having a mean lattice spacing of 3.06 μm (○). The error bars represent 95% confidence bounds on simulation results. Also shown for comparison are the mean collision probability assumed in the model, $\rho = R_g/a$, and the areal post density, d/a. The areal post density is not plotted in part c due to its much higher value relative to the simulation results.

under consideration. We introduce a second parameter $\mathrm{Pe}_{\mathrm{coil}}$, defined as follows:

$$\mathrm{Pe}_{\mathrm{coil}} = \frac{\mu_0 E \zeta N}{k_B T / R_g} \equiv \mathrm{Pe}_{\mathrm{chain}} \frac{R_g}{A} \tag{14}$$

$\mathrm{Pe}_{\mathrm{coil}}$ represents the ratio of the drag force to the thermal force acting on the chain in its equilibrium, coil configuration. An $O(1)$ value of $\mathrm{Pe}_{\mathrm{coil}}$ marks the onset of Gaussian chain stretching, whereas the chain configuration is dominated by thermal forces at lower values of $\mathrm{Pe}_{\mathrm{coil}}$.[13,22] For the systems under consideration, this transition occurs at an $O(0.1)$ value of $\mathrm{Pe}_{\mathrm{chain}}$. Consequently, for $O(0.1)$ or lower values of $\mathrm{Pe}_{\mathrm{chain}}$, the chain retains its coil configuration. The mobilities increase in this regime as the field strength is increased, since the dominant mechanism of chain motion gradually changes from thermal diffusion to convection by the field. Because of the near-absence of chain stretching, the probability of hooking collisions is very low. The apparent increase in collision probability suggested by Figure 6a,b in this regime is merely an artifact of its definition as the number of collisions per lattice spacing covered by the chain, since at low values of $\mathrm{Pe}_{\mathrm{chain}}$, the chain center of mass does not cover a significant distance. Moreover, the chain, by darting around obstacles without forming a hooked configuration, is able to satisfy the condition imposed by us to identify collisions that a portion of the chain be present in all four quadrants surrounding the obstacle center. For the same reason, the apparent decrease in the distance covered between successive collisions suggested by Figure 5a,b is also an artifact of the criteria adopted by us for its measurement.

In the regime where $\mathrm{Pe}_{\mathrm{coil}} \leq 1$, we may expect the approximation of the DNA coil by a rigid sphere of equivalent radius to be valid. The mobility and diffusivity of a particle in periodic and random lattices under the application of a field have been studied by Gauthier and Slater and Gauthier et al. via Monte Carlo simulations.[36,37] These authors found that the mobility and diffusivity of the particle remain constant independent of the field in the regime $\mathrm{Pe}_{\mathrm{coil}} \leq 1$, while the diffusivity exhibits a power-law dependence on $\mathrm{Pe}_{\mathrm{coil}}$ with an exponent of 2 for $\mathrm{Pe}_{\mathrm{coil}} > 1$, where $\mathrm{Pe}_{\mathrm{coil}}$ is now interpreted as the ratio of the force exerted by the field to the thermal force acting over a length scale equal to the particle dimension. Consistent with these findings in the regime $\mathrm{Pe}_{\mathrm{coil}} \lesssim 1$ or, equivalently, $\mathrm{Pe}_{\mathrm{chain}} \lesssim 0.1$, Figure 7 reveals that the dispersivity of the chain normalized with respect to its free solution value remains relatively unaffected by the field for $\mathrm{Pe}_{\mathrm{chain}} \lesssim 0.1$. The approximation of the chain by a rigid sphere is no longer valid as $\mathrm{Pe}_{\mathrm{chain}}$ is increased beyond this value. Figure 7 suggests a power-law dependence of dispersivity on the chain Peclet number for $\mathrm{Pe}_{\mathrm{chain}} > 0.1$, with an exponent of approximately 1.3. The faster-than-linear rise in dispersivity with the chain Peclet number is also manifested in Figure 4 and is attributed to the fact that while collisions become increasingly rare at high field strengths, those that do occur involve long holdup times.

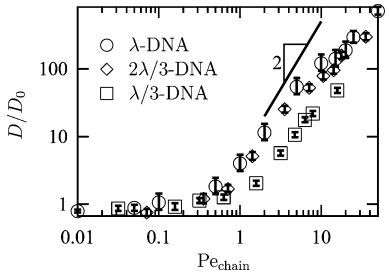

Figure 7. Dispersivity of λ-DNA (○), $2\lambda/3$-DNA (◇), and $\lambda/3$-DNA (□) normalized with respect to the free solution diffusion coefficient of a free draining chain, i.e., $D_0 = k_BT/(N\zeta)$, as a function of the Peclet number for λ-, $2\lambda/3$-, and $\lambda/3$-DNA, respectively, obtained by simulation in a self-assembled array of magnetic beads having a mean lattice spacing of 3.06 μm. The error bars represent 95% confidence bounds on simulation results. Above a Peclet number of 0.1 for each chain length, D/D_0 exhibits a power-law dependence on Pe_{chain} with an exponent of approximately 1.3. Also shown for comparison is a line of slope 2, representing the power-law dependence of the normalized diffusivity D/D_0 of a rigid particle on the field strength in a lattice of periodic obstacles.[37]

We are now in a position to evaluate the ability of the CTRW model to predict the behavior of the chain. The CTRW mechanism is not realized for $Pe_{coil} \sim O(1)$, owing to the rarity of hooking events, and consequently, the model fails in the regime $Pe_{chain} \sim O(A/R_g)$. The model is able to predict the dispersivity reasonably well, as depicted by Figure 4. However, the model fails to predict the minima in the mobility and the mean distance covered between successive collisions, instead predicting a monotonic decrease in mobility and a monotonic increase in the distance covered between collisions, respectively, beyond $Pe_{chain} = 1$, as illustrated by Figures 3 and 5. This failure of the model may be attributed in part to the use of a fixed collision probability $\rho = R_g/a$ regardless of the field strength. Consequently, the model does not account for the existence of a maximum in ρ at an $O(1)$ chain Peclet number. We also note that the dependence of ρ on the size of the chain is manifestly evident in Figure 6, rendering inaccurate the use of the areal post density d/a for ρ. In fact, the dependence on the size appears to be stronger than that assumed by eq 8, as suggested by the increase in the disparity between the simulation results and eq 8 as the chain size decreases. Equation 8 assumes a simple dependence on only two of four (or possible more) length scales relevant to the collision process, namely, the chain size, post size, lattice spacing, impact parameter,[15,16,18] and possibly others. Moreover, our use of eq 8 for the collision probability presupposes instantaneous chain relaxation to equilibrium and fails to take into account the reduction in the transverse radius of gyration and, hence, the chain cross-section transverse to the electric field direction following a collision at high field strengths. A further shortcoming of eq 8 is that it fails to take into account the dependence of the collision probability on the distortion of the electric field by the obstacles.[18]

Figure 8 provides a comparison between the resolution predicted by the model and that obtained from simulation data by means of eq 10 for each pair of chains as a function of the field strength (expressed in terms of Pe_λ). The mean velocity and dispersivity, measured in the long time limit after the chain has equilibrated in the array, are independent of the array length for a sufficiently long array. In the present study, we consistently employ a separation length of $L_s = 1$ cm, which is similar to the values used in prior studies.[3,34] The error bars for the simulation results were computed from the differential error analysis of eq 10, treating the velocities and dispersivities of the two species as independently measurable quantities. The model successfully predicts the nonmonotonic behavior of the

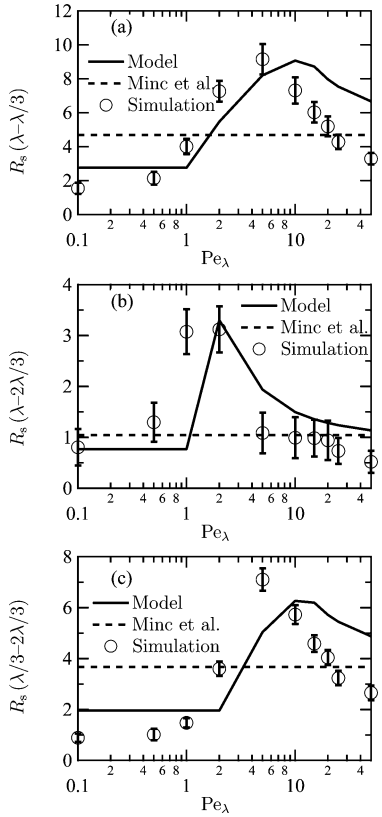

Figure 8. Separation resolution between (a) λ- and $\lambda/3$-DNA, (b) λ- and $2\lambda/3$-DNA, and (c) $\lambda/3$- and $2\lambda/3$-DNA as a function of Pe_λ calculated by simulation in a self-assembled array of magnetic beads having a mean lattice spacing of 3.06 μm (○) and that predicted by the model (—) for a separation length of $L_s = 1$ cm. The error bars represent 95% confidence bounds on simulation results. Also shown for comparison is the separation resolution predicted by the model of Minc et al. (- - - -).

resolution with respect to the field strength. The attainment of a high resolution is contingent on the existence of a low dispersivity for both chains and a large velocity difference between the chains. These conditions are met at an $O(1)$ value of Pe_λ. The decrease in the resolution at high field strengths may be attributed to the increase in dispersivity with the field strength. Furthermore, although the model fails to predict the existence of a minimum in the mobility, it is able to qualitatively capture the decline in the chain mobilities in the region $Pe_{chain} \sim O(1)$ and, consequently, the initial increase in resolution in this region.

Also depicted in Figures 3−5 and 8 are the results for the corresponding quantities predicted by Minc et al.[7] under the same conditions. The model of Minc et al. clearly fails to predict the field-dependence of the chain dynamics and, consequently, the nonmonotonic dependence of the resolution on the electric field strength observed in the simulations conducted in the present study, as well as in previous experimental work.[3] Quantitatively, as manifest in Figure 3, Minc et al. predict far lower values of the chain mobility than those observed in simulations, owing to their overestimation of the collision probability and the chain extension.

4.2. Varying Mean Lattice Spacings. Figures 9−12 provide comparisons between the simulation results and model predictions at varying lattice spacings, at a fixed field strength corresponding to $Pe_\lambda = 5$, with the error bars again representing 95% confidence bounds on the simulation results. The CTRW model is unable to predict the normalized mobility and dispersivity at a mean lattice spacing of 1.53 μm. The effective

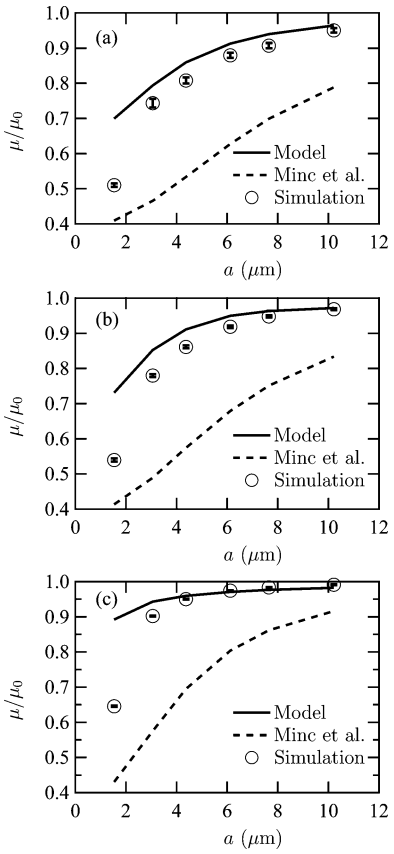

Figure 9. Normalized mobility of (a) λ-DNA, (b) $2\lambda/3$-DNA, and (c) $\lambda/3$-DNA as a function of the mean lattice spacing obtained by simulation in a self-assembled array of magnetic beads at $Pe_\lambda = 5$ (○), that predicted by the model (—), and that predicted by the model of Minc et al. (- - - -). The error bars represent 95% confidence bounds on simulation results.

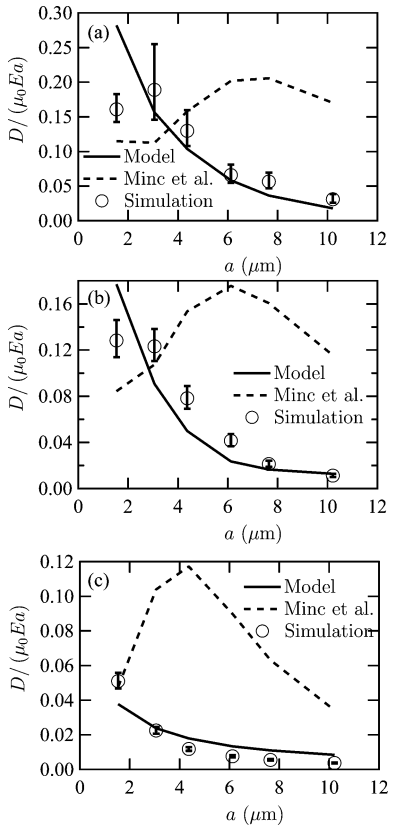

Figure 10. Normalized dispersivity of (a) λ-DNA, (b) $2\lambda/3$-DNA, and (c) $\lambda/3$-DNA as a function of the mean lattice spacing obtained by simulation in a self-assembled array of magnetic beads at $Pe_\lambda = 5$ (○), that predicted by the model (—), and that predicted by the model of Minc et al. (- - - -). The error bars represent 95% confidence bounds on simulation results.

mean pore size available to the chain in this array, $a - d = 0.53$ μm, is exceeded by the coil diameters of all three DNA chains under consideration. Equation 8 predicts an unphysical, diverging collision probability as a decreases to 0, leading to the divergence of the dispersivity [cf. eq 7] in this limit, while the mobility [cf. eq 6] approaches a constant value of $^2/_3$. The CTRW mechanism is not realized when $a - d \lesssim 2R_g$, and the mechanism is better described by the reptation model[5] or the entropic barrier model.[38] The CTRW model performs well at the remaining lattice spacings and is able to predict the asymptotic approach of the normalized mobility and normalized dispersivity to 1 and 0, respectively, as the lattice spacing increases.

As evident from Figure 12, the collision probability assumed in the CTRW model agrees well with the corresponding simulation results for λ-DNA and $2\lambda/3$-DNA. Figure 11 reveals that the mean distance covered between successive collisions as predicted by the model accords with simulation results for λ-DNA and $2\lambda/3$-DNA at mean lattice spacings below 7.65 μm. However, at mean lattice spacings of 7.65 and 10.21 μm, fewer than two collisions were observed to occur in as many as up to 50% of all simulated trajectories, which were excluded from the calculation of $\langle n \rangle a$. As a result, the simulation results do not reflect the increase in the distance between collisions predicted by the model under these conditions. The field strength at $Pe_\lambda = 5$ yields the values $Pe_{2\lambda/3} = 3.55$ and $Pe_{\lambda/3} = 1.58$. At these $O(1)$ values of Pe_{chain}, the collision probability reaches a maximum with respect to the Peclet number and is close to that predicted by eq 8 for λ-DNA and $2\lambda/3$-DNA, thus explaining the success of the model. The location of this maximum occurs at a higher value of Pe_{chain} for $\lambda/3$-DNA, as pointed out earlier. As a result, there is a large disparity between the collision probability predicted by eq 8 and the much lower values observed in simulations for $\lambda/3$-DNA. The corresponding predictions for the mean distance covered between collisions are exceeded by the results obtained from simulation. Collisions were rarely observed to occur at large lattice spacings for $\lambda/3$-DNA.

Figure 13 depicts the resolution predicted by the model and that obtained from simulation data for each pair of chains as a function of the lattice spacing. The error bars have been computed as before from the differential error analysis of eq 10. The CTRW model predicts the existence of a maximum in the resolution with respect to the lattice spacing and the decrease of the resolution to 0 at both small and large lattice spacings. In the regime $a - d > 2R_g$, the CTRW model correctly predicts the decrease in the resolution between λ-DNA and $\lambda/3$-DNA, and between $\lambda/3$-DNA and $2\lambda/3$-DNA, as the lattice spacing is increased. The quantitative differences between model predictions and simulation results may be attributed to the failure of the model to correctly describe the collision probability for $\lambda/3$-DNA. Again in the regime of its validity, the resolution predicted by the model between λ-DNA and $2\lambda/3$-DNA is close to that obtained from simulation within error bars. Unfortunately, it is not possible to conclusively identify the existence of a maximum in the resolution from the simulation data of Figure 13b, owing to the size of the error bars.

The predictions of Minc et al.,[7] also illustrated in Figures 9−11 and 13, do not adequately capture the chain dynamics with increase in the lattice spacing. As apparent from Figure 9, Minc et al. predict much lower values of the mobility than those

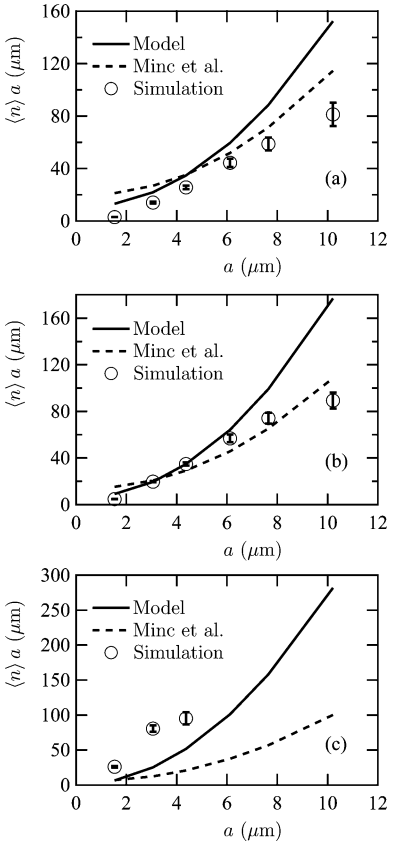

Figure 11. Mean distance covered between successive collisions by (a) λ-DNA, (b) $2\lambda/3$-DNA, and (c) $\lambda/3$-DNA as a function of the mean lattice spacing obtained by simulation in a self-assembled array of magnetic beads at $Pe_\lambda = 5$ (○), that predicted by the model (—), and that predicted by the model of Minc et al. (- - - -). The error bars represent 95% confidence bounds on simulation results. The simulation data shown for $\lambda/3$-DNA correspond to $a = 1.53$ μm , $a = 3.06$ μm, and $a = 4.37$ μm only, since collisions were found to occur in fewer than 10% of the simulated trajectories at larger values of the mean lattice spacing.

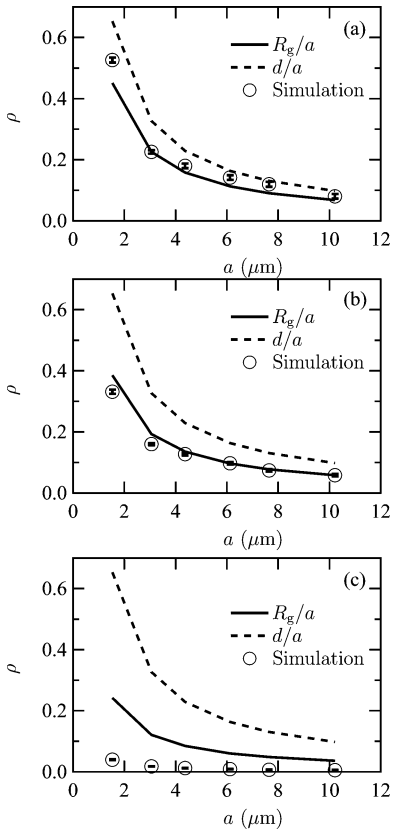

Figure 12. Mean collision probability ρ of (a) λ-DNA, (b) $2\lambda/3$-DNA, and (c) $\lambda/3$-DNA as a function of the mean lattice spacing, calculated from simulation as the number of chain−obstacle collisions per lattice column crossed by the chain center of mass at $Pe_\lambda = 5$ in a self-assembled array of magnetic beads. Also shown for comparison are the mean collision probability assumed in the model, $\rho = R_g/a$, and the areal post density, d/a.

observed in simulations. Moreover, as shown in Figure 10, they predict the existence of a maximum in the normalized dispersivity with respect to the lattice spacing, not seen to occur in simulations. Their predictions fail to reflect the rapid decline in the resolution with increase in the lattice spacing seen in the simulation data of Figure 13. At the field strength under consideration, the chains are relatively strongly stretched and the assumptions made by Minc et al.[7] regarding the holdup time and the collision probability, rather than their neglect of the field-dependence of chain extension, may be responsible for the discrepancies between their predictions and the simulation results.

5. Discussion

In the present study, we provide a generalization of the CTRW model of DNA dynamics in an array of obstacles[7] with account for the electric field dependence of the chain extension during collisions. We make use of a semiempirical expression recently developed from studies on chain collisions with single obstacles[21] for the holdup time during which the chain center of mass motion is impeded by the obstacle following a collision. In addition, we take into account the dependence of the collision probability on the chain size.

We evaluate the model by comparing its predictions with the results obtained from Brownian dynamics simulations of bead−spring models of λ-DNA, $2\lambda/3$-DNA, and $\lambda/3$-DNA in obstacle arrays. The use of a regular hexagonal lattice yields high mobilities approaching the free solution electrophoretic mobility, and hence, proves ineffective in achieving separation between chains of different sizes. Instead, we select a self-assembled array of magnetic colloids as being representative of arrays used in experimental studies.[2−4] These arrays are generated via Brownian dynamics simulations of magnetic colloids that interact with each other via a repulsive point dipolar potential and mutual hard-sphere exclusion in two dimensions.[23,24] Our studies are conducted in an array having a mean lattice spacing of 3.06 μm at several experimentally accessible electric field strengths and at a constant electric field strength equivalent to a Peclet number of $Pe_\lambda = 5$ at several values of the mean lattice spacing. Our neglect of hydrodynamic interactions in all simulations is partially justified by the screening of hydrodynamic interactions in complicated microchannel geometries. We also neglect the distortion of the electric field due to the presence of obstacles, a factor that may have adversely impacted our ability to accurately model the probability of chain−obstacle collision.[18]

Our simulation studies of chain dynamics at varying Peclet numbers enable the identification of three regimes demarcated by the chain Peclet number. The regime $Pe_{chain} \lesssim O(A/R_g)$ corresponds to the situation wherein thermal equilibrium has yet to be disturbed, i.e., the drag on the chain, $\mu_0 EN\zeta$, is exceeded by the thermal force k_BT/R_g acting on the chain in its equilibrium, coil configuration. Under such conditions, the formation of hooked chain configurations is unlikely and the mechanism of the CTRW model is not realized. The range $O(A/R_g) < Pe_{chain} \lesssim O(1)$ is associated with chain stretching in

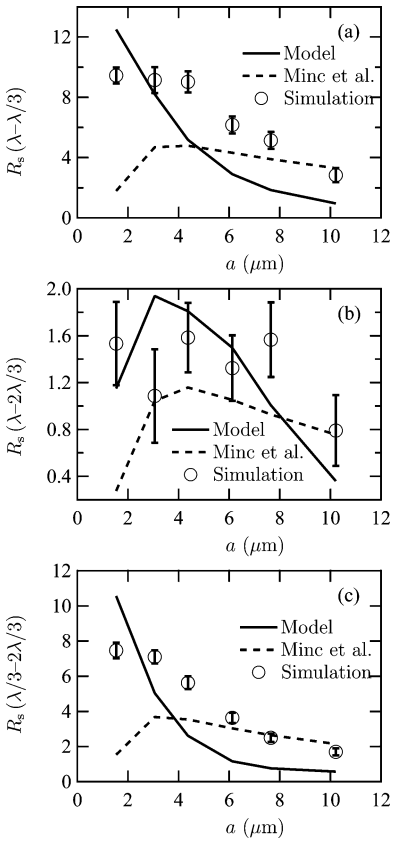

Figure 13. Separation resolution between (a) λ- and λ/3-DNA, (b) λ- and 2λ/3-DNA, and (c) λ/3- and 2λ/3-DNA as a function of the mean lattice spacing calculated by simulation in a self-assembled array of magnetic beads at $Pe_\lambda = 5$ (○) and that predicted by the model (—) for a separation length of $L_s = 1$ cm. The error bars represent 95% confidence bounds on simulation results. Also shown for comparison is the separation resolution predicted by the model of Minc et al. (- - - -)

the Gaussian regime, whereby the chain extension is well-described by the low-force limit of the Marko−Siggia formula.[22] The chain mobility reaches a minimum at an $O(1)$ value of Pe_{chain}, corresponding to the attainment of a maximum in the collision probability. For $Pe_{chain} \gg O(1)$, the chain extension is derived from the large-force limit of the Marko−Siggia law.[22] In this regime, the probability of chain−obstacle collision decreases and, consequently, the mobility increases. At the same time, the chain dispersivity increases with the field strength, owing to the fact that while collisions are rare, they involve long holdup times when they do occur. Further investigation of a wider range of chain sizes is required to conclusively establish the proposed dependence of these regimes on chain size.

The CTRW model, in failing to account for the dependence of the collision probability on the field strength, is unable to predict the existence of a minimum in the chain mobility with respect to the Peclet number. However, it satisfactorily predicts the increase in dispersivity with increasing field strength and the initial decline in the mobility at $O(1)$ values of the Peclet number, and consequently, is able to predict the existence of a maximum in the separation resolution with respect to the field strength. Under conditions of constant electric field strength, the CTRW model is able to provide reasonable predictions of the chain dynamics as the lattice spacing is varied in the regime of its applicability, when the mean pore size available to the chain in between obstacles exceeds the chain size.

The use of a constant collision probability, independent of the electric field strength, is an obvious weakness of the model. The model also does not account for the effect of the distortion of the electric field lines in the vicinity of the obstacles and neglects the dependence of the collision probability on other relevant length scales such as the impact parameter and the post size.[15,16,18] We emphasize that the collision probability assumed by us is justifiable only when the post diameter is small compared to the chain diameter. The influence of the post size on the collision probability bears further investigation by means of experiment or simulation wherein the post diameter is varied. Yet another source of error is the assumption that the chain instantaneously relaxes to a coil at the location of its leading end following a collision and subsequently moves at its free solution electrophoretic velocity $\mu_0 E$ until the next collision occurs.

Owing to the paucity of experimental studies on the systems under consideration, we are able to provide only limited comparisons with experiment. The nonmonotonicity of the separation resolution with respect to the electric field strength, as predicted by us, was observed by Minc et al. in studies on the separation of λ-DNA and 2λ-DNA chains.[3] These authors also observed the separation resolution to increase upon changing the lattice spacing from 3.8 to 4.1 μm. This observation, taken in conjunction with the decrease in resolution that must necessarily follow at large lattice spacings upon approaching the single-obstacle limit, renders the resolution nonmonotonic with respect to the lattice spacing. However, in the latter study, the obstacle diameters were concurrently changed from 1 to 1.4 μm, whereby the increase in resolution cannot conclusively be attributed to the increase in the lattice spacing. We are unable to confirm the existence of a maximum in the separation resolution with respect to the lattice spacing, as predicted by our model, owing to the size of the error bars associated with our simulation results.

Our findings shed light on the behavior of field-driven polymers in post arrays wherein the pore size is large compared to the coil size of the polymer. Moreover, our results successfully reflect the experimentally observed nonmonotonicity of the separation resolution with respect to the electric field strength and are expected to aid in the appropriate selection of parameters for the operation of obstacle arrays employed for the size separation of DNA chains and similar molecules.

Acknowledgment. We thank Dr. Ramin Haghgooie of Massachusetts General Hospital and MIT for providing us with the code for generating the magnetic colloid assemblies used in the present study and for several helpful discussions. This research used resources of the National Energy Research Scientific Computing Center, which is supported by the Office of Science of the U.S. Department of Energy under Contract No. DE-AC02-05CH11231. We gratefully acknowledge the support of NSF-NIRT Grant No. CTS-0304128 and NSF-CAREER Grant No. CTS-0239012 for this work.

References and Notes

(1) Volkmuth, W. D.; Austin, R. H. *Nature* **1992**, *358*, 600−602.
(2) Doyle, P. S.; Bibette, J.; Bancaud, A.; Viovy, J.-L. *Science* **2002**, *295*, 2237.
(3) Minc, N.; Futterer, C.; Dorfman, K. D.; Bancaud, A.; Gosse, C.; Goubault, C.; Viovy, J.-L. *Anal. Chem.* **2004**, *76*, 3770−3776.
(4) Minc, N.; Bokov, P.; Zeldovich, K. B.; Futterer, C.; Viovy, J.-L.; Dorfman, K. D. *Electrophoresis* **2005**, *26*, 362−375.
(5) Viovy, J.-L. *Rev. Mod. Phys.* **2000**, *72*, 813−872.
(6) Inatomi, K.; Izuo, S.; Lee, S.; Ohji, H.; Shiono, S. *Microelectron. Eng.* **2003**, *70*, 13−18.
(7) Minc, N.; Viovy, J.-L.; Dorfman, K. D. *Phys. Rev. Lett.* **2005**, *94*, 198105.
(8) Dorfman, K. D. *Phys. Rev. E* **2006**, *73*, 061922.

(9) Scher, H.; Lax, M. *Phys. Rev. B* **1973**, *7*, 4491−4502.
(10) Hughes, B. D. *Random Walks and Random Environments, Volume I: Random Walks*; Clarendon: Oxford, U.K., 1995.
(11) Popelka, S.; Kabatek, Z.; Viovy, J.-L.; Gas, B. *J. Chromatogr., A* **1999**, *838*, 45−53.
(12) Mohan, A.; Doyle, P. S. *Macromolecules* **2007**, *40*, 4301−4312.
(13) Brochard-Wyart, F. *Europhys. Lett.* **1995**, *30*, 387−392.
(14) Nixon, G. I.; Slater, G. W. *Phys. Rev. E* **1994**, *50*, 5033−5038.
(15) Sevick, E. M.; Williams, D. R. M. *Phys. Rev. Lett.* **1996**, *76*, 2595−2598.
(16) Saville, P. M.; Sevick, E. M. *Macromolecules* **1999**, *32*, 892−899.
(17) Sevick, E. M.; Williams, D. R. M. *Europhys. Lett.* **2001**, *56*, 529−535.
(18) Randall, G. C.; Doyle, P. S. *Phys. Rev. Lett.* **2004**, *93*, 058102.
(19) Randall, G. C.; Doyle, P. S. *Macromolecules* **2005**, *38*, 2410−2418.
(20) Randall, G. C.; Doyle, P. S. *Macromolecules* **2006**, *39*, 7734−7745.
(21) Kim, J. M.; Doyle, P. S. *Macromolecules*, in press.
(22) Marko, J. F.; Siggia, E. D. *Macromolecules* **1995**, *28*, 8759−8770.
(23) Haghgooie, R.; Doyle, P. S. *Phys. Rev. E* **2004**, *70*, 061408.
(24) Haghgooie, R.; Doyle, P. S. *Phys. Rev. E* **2005**, *72*, 011405.
(25) Zumofen, G.; Klafter, J. *Phys. Rev. E* **1993**, *47*, 851−863.
(26) Long, D.; Dobrynin, A. V.; Rubinstein, M.; Ajdari, A. *J. Chem. Phys.* **1998**, *108*, 1234−1244.
(27) Chen, Y.-L.; Graham, M. D.; de Pablo, J. J.; Randall, G. C.; Gupta, M.; Doyle, P. S. *Phys. Rev. E* **2004**, *70*, 060901.
(28) Hsieh, C. C.; Li, L.; Larson, R. G. *J. Non-Newtonian Fluid Mech.* **2003**, *113*, 147−191.
(29) Underhill, P. T.; Doyle, P. S. *J. Non-Newtonian Fluid Mech.* **2004**, *122*, 3−31.
(30) Jendrejack, R. M.; de Pablo, J. J.; Graham, M. D. *J. Chem. Phys.* **2002**, *116*, 7752−7759.
(31) Doi, M.; Edwards, S. F. *The Theory of Polymer Dynamics*; Clarendon: Oxford, U.K., 1986.
(32) Heyes, D. M.; Melrose, J. R. *J. Non-Newtonian Fluid Mech.* **1993**, *46*, 1−28.
(33) DeGroot, M. H.; Schervish, M. J. *Probability and Statistics*; Addison-Wesley: New York, 2002.
(34) Patel, P. D.; Shaqfeh, E. S. G. *J. Chem. Phys.* **2003**, *118*, 2941−2951.
(35) Allen, M. P.; Tildesley, D. J. *Computer Simulation of Liquids*; Oxford University Press: Oxford, U.K., 1987.
(36) Gauthier, M. G.; Slater, G. W. *J. Chem. Phys.* **2002**, *117*, 6745−6756.
(37) Gauthier, M. G.; Slater, G. W.; Dorfman, K. D. *Eur. Phys. J. E* **2004**, *15*, 71−82.
(38) Muthukumar, M. *J. Non-Cryst. Solids* **1991**, *131*−*133*, 654−666.

MA071354E